J Mater Sci: Mater Electron (2021) 32:11989–12000

Fabrication of hierarchical CuO architectures displaying the (111) facets-enhanced superior fenton-like degradation of organic dyes

Hanmei Hu[1,*], Hong Yu[1], Kangze Ding[1], Zanzan Jiang[2], Yaping Liao[2], Xinqing Ge[1], Mei Sun[1], and Chonghai Deng[2,*]

[1] Anhui Province Key Laboratory of Advanced Building Materials, Anhui Jianzhu University, Hefei 230601, China
[2] Department of Chemical and Materials Engineering, Hefei University, Hefei 230601, China

Received: 19 November 2020
Accepted: 23 March 2021
Published online: 15 April 2021

ABSTRACT

Three types of hierarchical CuO architectures with the varying (111) facets exposure were controllably fabricated by a microwave-assisted wet chemical route. The products were characterized by X-ray diffraction (XRD), field emission scanning electron microscopy, transmission electron microscopy (TEM), and high-resolution TEM. The results demonstrate that the monoclinic hierarchical pumpkin-like CuO (p-CuO) crystals are self-assembled by 1D nanoribbons primarily exposed (111) lattice planes with diameters of 6–7 nm. Specifically, the XRD peak intensity ratios of $I_{111}/I_{\_\ 111}$ were calculated to be 1.38 for p-CuO, which is much larger than that of the other shuttle-like CuO (s-CuO) (1.01) and CuO microspheres (m-CuO) (0.92). The possible growth mechanism for the three kinds of CuO microstructures was proposed. Interestingly, it is a finding for the first time that the Fenton-like catalytic activities of the as-prepared CuO catalysts are closely relied on their preferential (111) facets exposure, in which the order of degradation rates of RhB, MB, and MO accords with the following: p-CuO > s-CuO > m-CuO. Significantly, the decoloring efficiency of RhB over p-CuO in the assistant of H_2O_2 was up to 93.7% within the initial 1 min, and the total removal rate reached 98.5% after 5 min, exhibiting the rapid and superior Fenton-like catalysis activity.

1 Introduction

Nowadays, industrial wastewater has become a major threat to ecosystem and human beings. Organic dye-containing wastewater contains a large amount of toxic and recalcitrant pollutants, resulting in increased risk in the incidence of bladder cancer [1]. At the same time, considerable effort has been paid by scientists and engineers to develop many technologies for water and air purification. Advanced oxidation process (AOP) is based on the in situ generation of high oxidative reactive hydroxyl radicles

Address correspondence to E-mail: hmhu@ustc.edu; chdeng@mail.ustc.edu.cn

https://doi.org/10.1007/s10854-021-05829-2

(·OH), which can unselectively decompose the hazardous organic pollutants into inorganic minor molecules such as CO_2 and H_2O [2–5]. As one of the AOP family, Fenton catalysis process has been applied in the practical industrial wastewater treatment. Conventionally, the homogeneous Fenton catalysis reaction usually adopted ferrous salts (Fe^{2+}) as co-catalysts to activate hydrogen peroxide (H_2O_2), thereby producing the active species ·OH [6, 7]. Although the classic Fe^{2+} Fenton system has the advantages of high efficiency, simplicity, maneuverability, and non-toxicity, there were serious problems including limitation by rigorous working pH range, long operation time, and difficult recovery. Therefore, the heterogeneous Fenton-like catalysts have come up, which are composed of Fe-based transition metal oxides and composites, such as $BiFeO_3$ [8], FeOCl [9], Fe_3O_4 and Fe_3O_4@SiO_2 [10, 11], Fe_3O_4@-void@TiO_2 [12], Pd/PdO/Fe_2O_3 [13], Cu-doped α-FeOOH [14], $CuFe_2O_4$@C_3N_4 [15], and Ag_3PO_4@-$NiFe_2O_4$ [16]. Recently, other non-ferrous Fenton-like catalysts have also been developed on the basis of Mn, Cu, and Co metal elements [17] such as Mn_3O_4 [18], CuS [19, 20], and $Co_xMn_{3-x}O_4$ compounds [21]. In addition, extra physical fields were often used to apply in the catalytic reaction in order to enhance catalytic efficiency, including photo- [22], electro- [5], cavitation- [23], and microwave-assisted processes [24].

Cupric oxides (CuO), as a semiconductor with a direct band gap of 1.2 eV, have attracted great attention by their unique physiochemical properties and potential application, such as sensing materials [25], Li-ion batteries [26, 27], supercapacitor [28], solar cells [29], and photocatalysts [30, 31]. It is well known that three-dimensional (3D) hierarchically structured architectures can provide a direct bridge between the nanoscale blocks and the macroscale world, which often embody the high efficiency of structure–activity relationship. For example, porous CuO microspheres with a sheet-like subunit-assembled micro/nanostructure manifested enhanced Li storage property [26]. Hierarchical CuO cauliflowers constructed by nanoflakes revealed superior catalytic activity for the degradation of Rhodamine B [30]. CuO microflowers composed of 2D nanosheets exhibited a broad-spectrum anti-bacterial activity [32]. Urchin-like core–shell CuO assembled by nanorods demonstrated a wide biosensor capability toward H_2O_2 [33]. CuO microstructures connected by intercrossed nanosheets gave high performance when applied as anode for lithium-ion battery [34]. Hollow CuO microflowers constructed by nanoparticle-based irregular petals showed improved catalytic property for the synthesis of organosilane [35]. And CuO architectures constructed by nanosheets exhibited the non-enzymatic glucose detection and ethanol gas-sensing property [36, 37]. To the best of our knowledge, most of the reported hierarchical CuO architectures for the high physicochemical property were mainly built by 2D sheet-like nanoblocks, yet 3D CuO architectures with a 1D nanounit-based micro/nanostructure are rarely reported in the literature [33, 38]. Specifically, despite a few publications on CuO displaying excellent Fenton-like catalytic properties [39, 40], so far there are no publication on the (111) crystal surface-enhanced Fenton-like catalytic activity of CuO architecture.

Herein, three types of 3D hierarchical CuO architectures with varying degrees of exposed (111) facets, that is, pumpkin-like CuO (p-CuO), shuttle-like CuO (s-CuO), and CuO microspheres (m-CuO), are controllably fabricated by a facile microwave-assisted wet chemical process. The 3D monoclinic p-CuO architectures are assembled by 1D nanoribbons with preferential exposed (111) lattice planes. As the efficient peroxidase-like catalysts, the enhanced AOP catalytic activities were evaluated to degrade three organic dyes (RhB, MB, and MO) over CuO catalysts with the assist of H_2O_2 in the dark. To date, it is a first time that the present work may disclose the structure–activity relationship between the Fenton-like activity and the preferential orientation of (111) facets of CuO nanocrystal.

2 Experimental

2.1 Sample preparation

Copper acetate monohydrate ($Cu(CH_3COO)_2{\cdot}H_2O$), monoethanolamine (C_2H_7NO, MEA), rhodamine B (RhB), methylene blue (MB), methyl orange (MO), and absolute ethanol were analytical grade (AR) purity and purchased from Sinopharm Chemical Reagent Company. All the chemicals were used as received without any further purification. Distilled water was used for the preparation of solutions.

The microwave-assisted aqueous chemical reactions were implemented in a locally supplied

microwave oven (Galanz D80D23N1P-T7 (B0), 2.45 GHz, maximum power 800 W). In a typical procedure, a 30 ml aqueous solution of MEA was added into 30 ml solution of $Cu(CH_3COO)_2{\cdot}H_2O$ (0.400 g) under continuous stirring for several minutes. The mixture reaction system was covered with a piece of PE film and then placed in a domestic microwave oven. After microwave irradiation was performed under low power for 30 min, the mixture was cooled naturally to room temperature. The resulting black precipitate was filtered and washed with distilled water and absolute ethanol for several times to remove residuals, and dried in a vacuum at 60 °C for 8 h. While the dosage of MEA (V_{MEA}) was introduced 0.1, 0.3, and 0.5mL in the synthesis, the collected CuO samples were donated as p-CuO, s-CuO, and m-CuO, respectively.

2.2 Characterization

The X-ray diffraction pattern of the as-prepared products were obtained by X-ray diffractometer (XRD, Rigaku TTR-III, λ = 1.5418 Å, 18 KW) using CuKα radiation. The surface morphologies and sizes of CuO samples were measured on a field emission scanning electron microscope (FESEM, Sirion-200) and a high-resolution transmission electron microscope (HRTEM, JEOL, JEM-2010). The BET surface areas were analyzed by nitrogen (N_2) adsorption with an Autosorb-iQ automatic surface area and pore analyzer. All the samples were degassed at 200 °C for 2 h prior to the N_2 adsorption measurements.

2.3 Fenton-like catalytic activity

Fenton-like catalytic activity tests were performed under atmospheric pressure, by shaking the beaker in a thermostat water bath with a temperature of 25 °C in the dark. Three kinds of colored organic dyes including RhB, MB, and MO were chosen as molecular probes to examine the catalysis performance. In the typical experiment, 30 mg of CuO catalyst was added to 50 mL of 10 mg/L RhB solution. Prior to the introduction of H_2O_2, the suspension was stirred continuously for 60 min to establish an adsorption–desorption equilibrium. The decolorization reaction proceeded in the thermostat water bath by shaking slowly and adding 0.5 mL of H_2O_2 (m/m, 30%). In the given time intervals, about 3–4 mL of suspension was sampled and centrifuged immediately to remove the powders. The concentration of aqueous dye left in the solution was analyzed using an UV-5500PC spectrophotometer.

3 Results and discussion

3.1 Characterization

Three types of CuO samples (p-CuO, s-CuO, and m-CuO) were controllably synthesized by adjusting the amount of 0.1, 0.3, and 0.5 mL MEA, respectively. The morphologies and sizes of the as-prepared products were investigated by FESEM and TEM. As shown in Fig. 1a, the panoramic picture revealed that p-CuO products are composed of the uniform pumpkin-like architectures with sizes of 600–1000 nm. From the high magnification image given in Fig. 1b, it can be distinctly observed that the architectures are assembled by numerous 1D ribbon-like nanounits, accompanying with various concave–convex rough surfaces. From the TEM images of Fig. 1c, it was confirmed that p-CuO sample is solid in nature, and lots of primary nanoribbons are predominantly aligned toward the center of the structure (inset). The high-resolution TEM (HRTEM) image is shown in Fig. 1d. It is observed that the diameters of the ribbon-like nanounits are measured to be about 6–7 nm. The straight and parallel lattice fringes indicate the high crystalline feature. By careful analysis of a single nanoribbon (inset), the regular spacing of lattice planes was calculated to be 0.234 nm, which is in good agreement with (111) lattice planes of monoclinic CuO, being consistent with CuO nanorod reported by Manna [44]. The FESEM images of s-CuO sample obtained with 0.3 mL MEA are shown in Fig. 1e. It can be seen that the products are mainly composed of large quantities of shuttle-like structures with long axis of 300–600 nm and short axis of 80–120 nm. Additionally, a few multigongal branching-off shuttles were found in the products. Furthermore, the architectures were also aggregated by numerous tiny nanograins, having the rough and protrusive surface (inset). Figure 1f presented the morphologies of m-CuO sample yield with 0.5 mL MEA. Obviously, the uniform and monodispersed products consisted of isotropic spherical structures with the diameters of 0.6–1.2 μm. From an enlarged FESEM image (inset), it also displayed that the

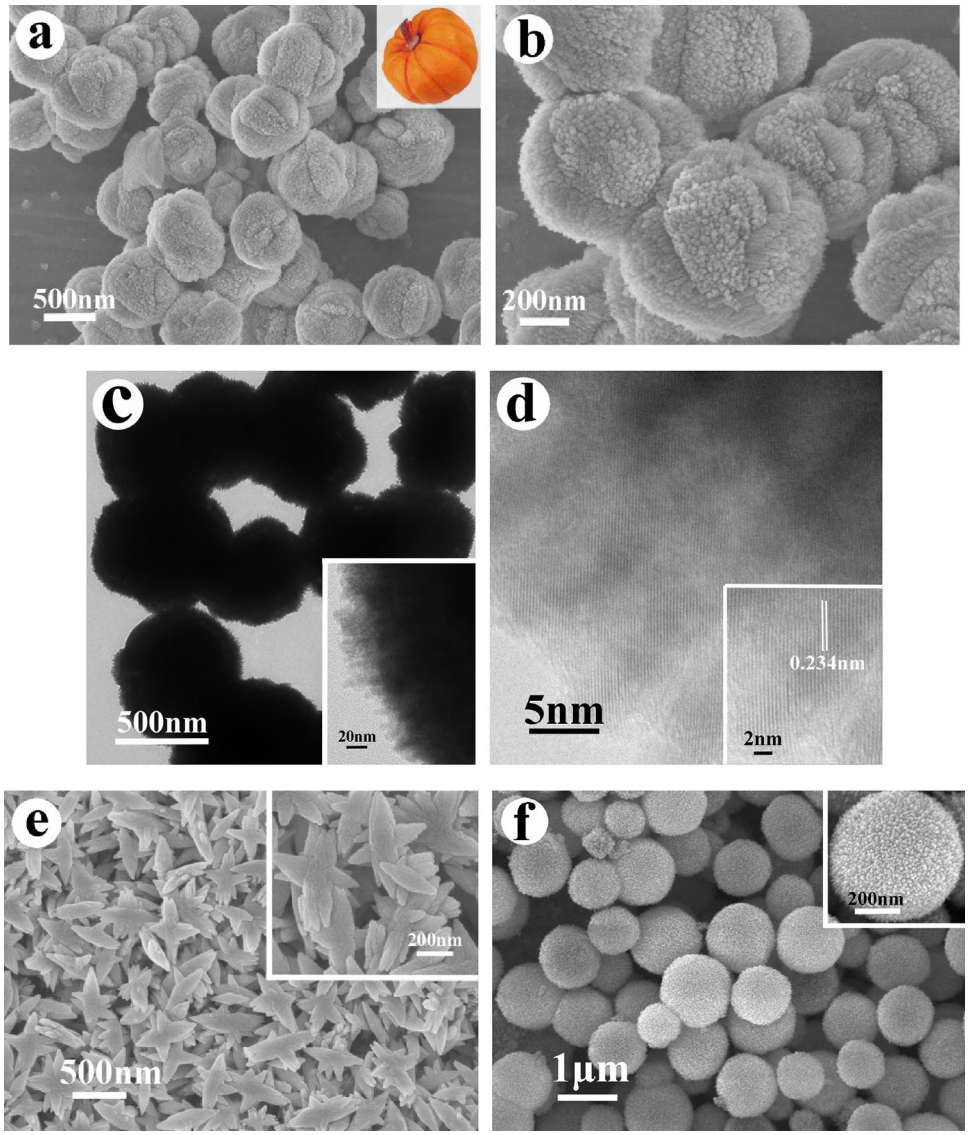

Fig. 1 **a** and **b** FESEM, **c** TEM, and **d** HRTEM images of p-CuO and **e**, **f** FESEM images of s-CuO and m-CuO, respectively

microspheres are assembled by the radial rod-like nanoparticles, having porous and protrusive surface.

The purity and crystallinity of the as-synthesized samples were determined by X-ray diffraction (XRD). The typical XRD patterns of three kinds of CuO products are displayed in Fig. 2a. All the diffraction peaks can be indexed to the monoclinic phase of CuO, consistent with the standard data from JCPDS card No. 05-0661. No characteristic peaks from impurities such as Cu and Cu_2O were detected, indicating high purity of the as-obtained samples. Besides, the relatively broader diffraction peaks suggested that the smaller crystallite size for CuO nucleus formed at the pregnancy stage of microwave irradiation. By further careful analysis, it is an interesting finding that the relative intensities of (111) and (− 111) peaks of three kinds of CuO products are orderly fluctuant. The peak intensity ratios (R) of I_{111}/I_{-111} were calculated to be 1.38, 1.01, and 0.92 for p-CuO, s-CuO, and m-CuO, respectively, as represented in Fig. 2b. The values of R successively decreased indicated that the CuO crystal orientations could be regulated by the adding dosages of MEA in the crystal growth process. Among them, p-CuO possessed the highest ratios of I_{111}/I_{-111}, suggesting the largest exposure proportion of (111) crystal surface, which could be responsibile for its ultrafast and superior Fenton-like catalytic activity toward the degradation of organic dyes.

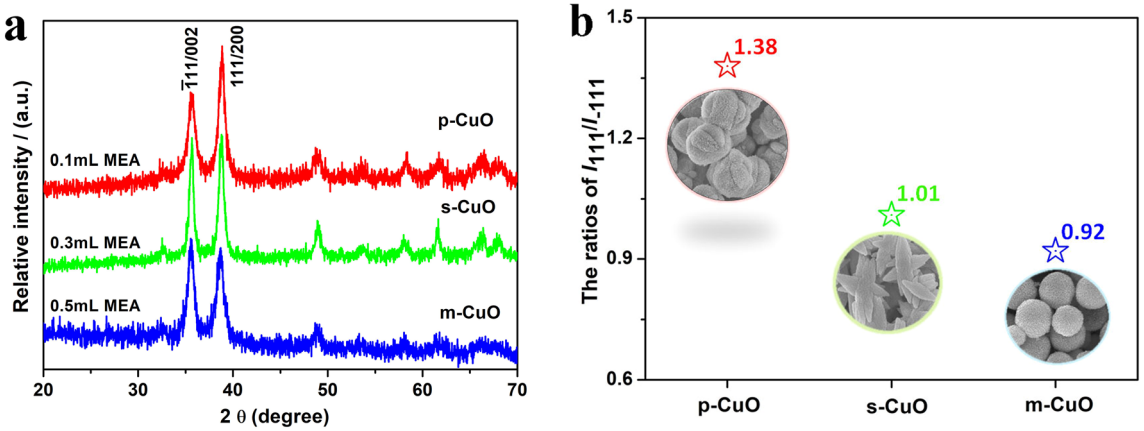

Fig. 2 **a** Typical XRD patterns and **b** the intensity ratios of I_{111}/I_{-111} of the as-prepared samples

3.2 Growth mechanism

The microwave-assisted wet chemical reaction was introduced to fabricate three kinds of CuO architectures. As is known, while the aqueous reaction was heated by microwave irradiation, the temperature and concentration gradients and lag effect of reaction can be avoided, thereby providing a uniform environment for rapid and homogeneous nucleation [41].

In this work, the organic alkali monoethanolamine (MEA) was employed as the complexing agent for the controllable synthesis of CuO architectures. While MEA was introduced into the Cu^{2+} ions solution, MEA can coordinate firstly with Cu^{2+} ions to form homogeneous Cu^{2+}-MEA complexes solution at room temperature [Eq. 1]. As soon as the reaction solution was heated by microwave irradiating, MEA molecules hydrolyze in aqueous solution and produce NH_3 [Eq. 2], which can drive the preformed Cu-MEA complexes to release dissociative free Cu^{2+} ion. Along with hydrolysis the hydroxide anions (OH^-) are generated [Eq. 3], the new-dissociated Cu^{2+} reacts with OH^- to form tetrahydroxocuprate anions $Cu(OH)_4^{2-}$ [Eq. 4]. Thereafter, the configurational ions $Cu(OH)_4^{2-}$ rapidly dehydrolyze to generate CuO nuclei under the microwave irradiation [Eq. 4]. All the main chemical reactions for the synthesis of three kinds of CuO architectures *via* the microwave-assisted aqueous chemical process may be expressed as follows:

$$Cu^{2+} + MEA \leftrightarrow Cu\text{ - }MEA\ complexes \quad (1)$$

$$HO(CH_2)_2NH_2 + H_2O = HO(CH_2)_2OH + NH_3 \quad (2)$$

$$NH_3 + H_2O = NH_4^+ + OH^- \quad (3)$$

$$Cu^{2+} + 4OH^- = Cu(OH)_4^{2-} \quad (4)$$

$$Cu(OH)_4^{2-} = CuO + H_2O + 2OH^- \quad (5)$$

In order to further understand the growth mechanism of p-CuO, the time-dependent experiments were performed. Figure 3 shows the FESEM images of the products obtained at different reaction stages. While the irradiation time was 5 min, lots of irregular ellipsoid-shaped CuO agglomerates assembled by tiny nanograins were collected (Fig. 3a). As the reaction time was up to 10 min, the relatively regular ellipsoid-shaped CuO agglomerates were formed (Fig. 3b). After the heating time extended to 20 min, the ripe ellipsoid-shaped CuO with pumpkin prototype were generated during the secondary growth (Fig. 3c). After the reaction time was increased up to 30 min, uniform maturity pumpkin-like CuO microstructures aggregated by tiny nanoparticles were fabricated finally on a large scale (Fig. 2a and b).

Based on the above control tests, an oriented aggregation growth mechanism can be proposed for the formation of p-CuO architectures. At first, under the microwave irradiation, numerous CuO primary nuclei are quickly generated and grown in the aqueous condition. In order to decrease the surface

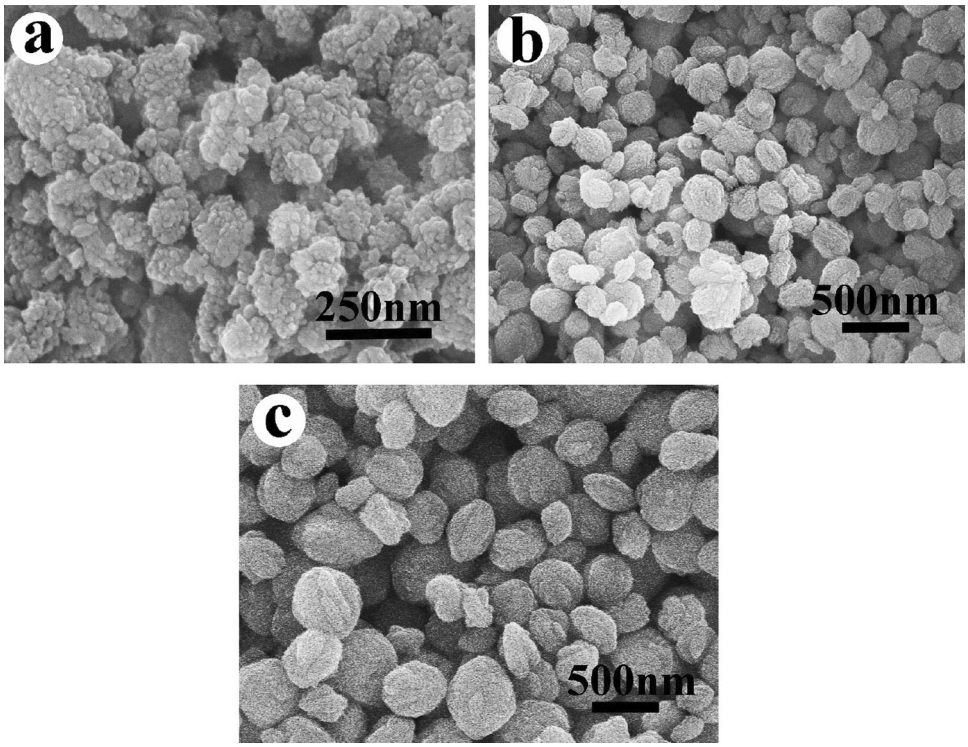

Fig. 3 FESEM images of CuO products obtained by adding 0.1 mL MEA at different growth stages: **a** 5 min, **b** 10 min, **c** 20 min

Gibbs energy, the preformed tiny nanograins pile up to aggregate ellipsoid-shaped CuO agglomerates. Next, secondary nucleation and growth can take place and grow out of pumpkin petals on the particles surface with the concave–convex active sites. Afterwards, CuO nanoparticles grew into nanoribbons with the special crystal face orientation with the crystal growing and Ostwald ripening. And the complete pumpkin-like CuO architectures were yield on the basis of the nanoribbons gradually self-aligned perpendicularly to the center.

According to the FESEM and XRD analysis of the three types of CuO products, it can be deduced that MEA plays an important role in the morphology and crystal orientation of CuO crystals. While the dosage of MEA was lowest (0.1 mL), all of MEA react with Cu^{2+} ions to form Cu^{2+}-MEA complexes and almost no free MEA molecules remained in the reaction solution. Thus, once the microwave heating starts, the Cu^{2+}-MEA complexes dissociated the free MEA molecules, which further hydrolyzed to generate OH^{-} ions. After suffering from nucleation, aggregation, and secondary growth, pumpkin-like CuO (p-CuO) architectures were formatted. While the dosage of MEA was increased (0.3 mL), apart from appropriate MEA molecules coordinate with Cu^{2+} ions to form Cu^{2+}-MEA complexes, superfluous free MEA molecules in the solution would adsorb onto the new-generated CuO crystal nuclei, tending to oriented attachment and assemble 1D structure. After the secondary nucleation and crystal growth, thereby the shuttle-like CuO (s-CuO) architectures are formed. While too much MEA (0.5 mL) was added, superfluous MEA may adsorb around the surfaces of CuO nuclei to form aggregates similar to en-capped nanoclusters [41], which drastically hindered the crystal orientation growth and uttermost decrease specific surface energy. Then with the isotropous slow growth and ripening, the intact CuO microspheres (m-CuO) were finally obtained. The possible schematic illustration of evolution processes of CuO structures with different morphologies are illustrated in Scheme 1. Honestly, the exact mechanism of the MEA-tailored formation of the CuO architectures is still under investigation. But as a matter of fact, based on the values of R (inset in the top right corner), it can be confirmed that the MEA molecules are apt to adsorb onto the (111) crystal surface of CuO nanocrystals, thereby retarding the oriented growth along (111) surface.

3.3 Fenton-like catalytic performance

The Fenton-like catalytic activities of three kinds of CuO micro/nanostructures were evaluated by the degradation of organic dyes in the dark. The dyes of RhB, MB, and MO were employed as molecular probes. Figure 4a displays the changes of the absorption spectra of RhB solution in the presence of p-CuO with the assistant of H_2O_2. The main absorption peak is located at 554 nm, which corresponded to RhB molecules. It was unexpected that the characteristic absorption peak diminishes sharply in the first minute, and almost disappears within 5 min, indicating the complete degradation through the Fenton-like catalytic process. The corresponding photograph images of RhB solution are given in the inset of Fig. 4a. The intense pink color of the starting solution rapidly fades, and became colorless and transparent only after 5 min. Figure 4b shows the time profiles of the degradation rates of RhB dye over the three different CuO catalysts under the control catalytic condition. Significantly, the decoloring rate over p-CuO with the help of H_2O_2 reached 93.7% within the initial 1 min, and after 5 min the decoloring rate achieved 98.5%, exhibiting the prompt and high efficient catalytic activity. For comparison, only in the presence of H_2O_2 without p-CuO, the degradation rate of RhB was 12.7% within 40 min. On the contrary, the decoloring of RhB was almost negligible over p-CuO in the absence of H_2O_2. Moreover, the corresponding decoloring rates over s-CuO and m-CuO with the help of H_2O_2 were nearly 90% and only 26.9% within 5 min, and reached about 98 and 65% until to 40 min later, respectively. Thus, a conclusion can be drawn that p-CuO architectures with dominantly exposed (111) facets display the fastest and highest Fenton-like catalytic ability for the degradation of RhB dye among CuO catalysts. Furthermore, the time profiles of the degradation rate of MB and MO over three CuO catalysts are given in Fig. 4c and d, respectively. The decoloring efficiencies of MB and MO over p-CuO with H_2O_2 reached up to 96.3 and 96.0% within 10 min, respectively, which remained significantly higher than that of s-CuO (41.2 and 54.8%) and m-CuO (19.5 and 17.2%) under the same experimental condition. Thus, the order of catalytic decomposing of three kinds of organic dyes over the three types of CuO catalysts accords to the following: p-CuO > s-CuO > m-CuO, which was in close agreement with the values of I_{111}/I_{-111} of CuO crystals. As is known, the specific surface area of nanomaterials is closely related to their physicochemical properties. The specific surface areas of three kinds of CuO samples were measured as 35.9822, 47.8568, and 29.9372 m^2/g for p-CuO, s-CuO, and m-CuO, respectively, indicating that the specific surface area of CuO catalyst is not the dominant factor on the peroxidase-like catalytic activity in the present system. Therefore, it is can be deduced that the different Fenton-like catalytic activities toward the degradation of RhB, MB, and MO over the as-prepared CuO samples dominantly depend on the exposure proportion of CuO (111) crystal surface.

The recycled catalytic experiments for the decomposing of RhB over p-CuO were further operated.

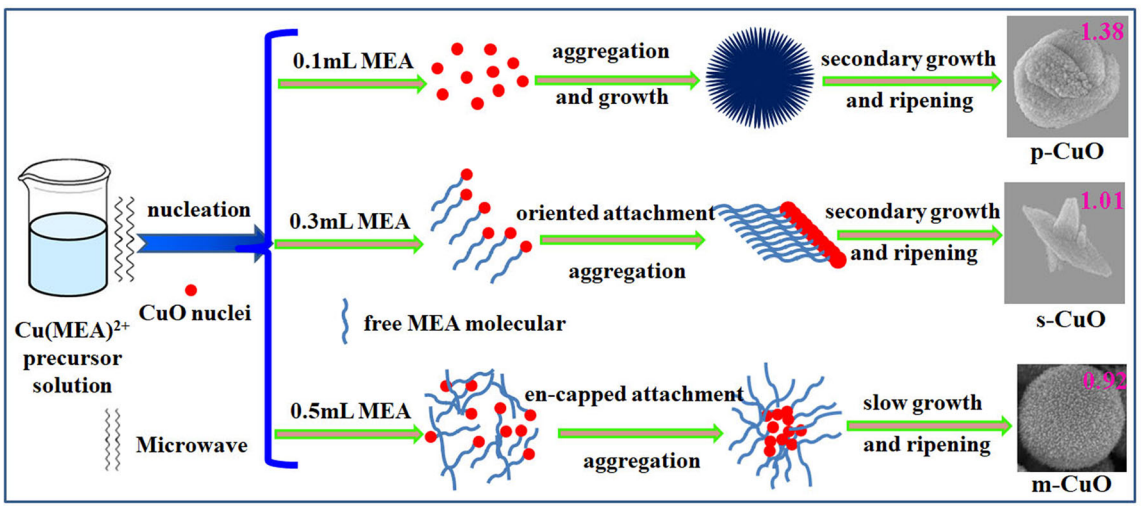

Scheme 1 Possible formation processes of CuO architectures with different morphologies

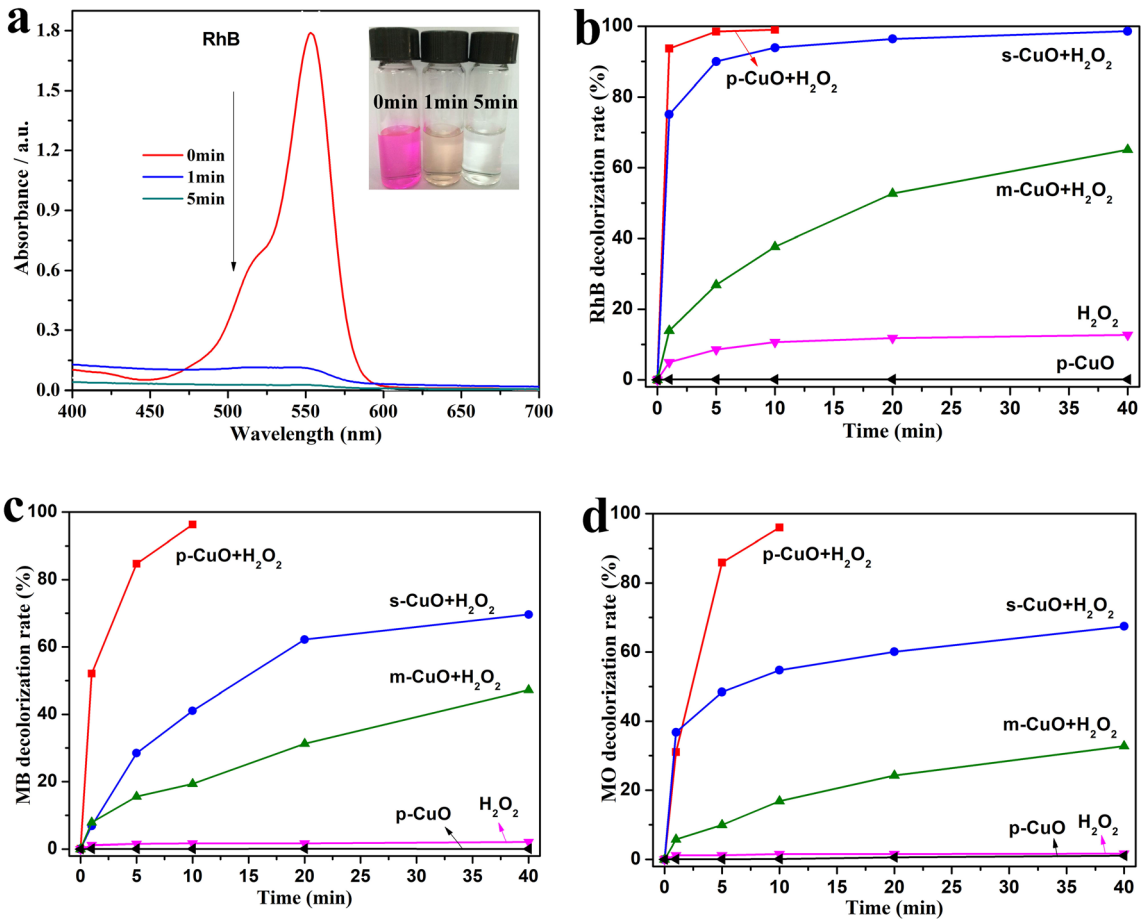

Fig. 4 **a** Absorption spectra of Fenton-like degradation of RhB over p-CuO with H_2O_2 in the dark, **b**–**d** Time profiles of the decoloration efficiencies of dyes (**b** RhB, **c** MB, and **d** MO) under different comparing conditions

Figure 5a shows the results of five cyclic tests in the degradation of RhB of over p-CuO with the help of H_2O_2 within 5 min. It was clear that the degradation rates gradually decreased with the increase of cycle numbers, and it maintained 69% after five recycles. Specially, the recycled p-CuO (herein named as r-CuO) was further characterized by XRD and FESEM. As shown in Fig. 5b, even if the XRD pattern of r-CuO was still indexed to the monoclinic phase of CuO (JCPDS 05-0661), obviously the original (111) crystal plane with dominant orientation almost disappeared. The peak intensity ratio of I_{111}/I_{-111} was calculated to be nearly 1.00, which was much lower than that of the fresh p-CuO (1.38). Furthermore, from the corresponding FESEM image (inset), the recycled sample was mainly composed of nanoplate-based CuO aggregates rather than the original nanoribbon-based p-CuO. Based on the above results, it can be illustrated that p-CuO nanocrystals suffer from the secondary crystallizing to transform r-CuO aggregated by nanoplate during the Fenton-catalytic process. Based on all the above catalytic experimental results, a hypothesis can be proposed that the superior Fenton-like catalytic activity of p-CuO is majorly ascribed to the dominantly exposed high-energy (111) crystal surface of CuO crystals.

The possible catalytic process of p-CuO architectures is shown in Scheme 2. At first, Cu^{2+} in the high-energy (111) crystal surface are reduced by H_2O_2 adsorbed on the crystal surface to generate Cu^{+} and ·OOH radicals. Cu^{2+} can further react with ·OOH radicals to produce Cu^{+} and O_2. Subsequently, the newly produced Cu^{+} are subsequently oxidized by H_2O_2 to yield Cu^{2+} again and the high reactive ·OH species. The photocorrosion reactions of copper oxide upon illumination with the aid of photoexcited charges have been studied comprehensively by Toe et al. [42]. Thereafter, the newly generated ·OH could

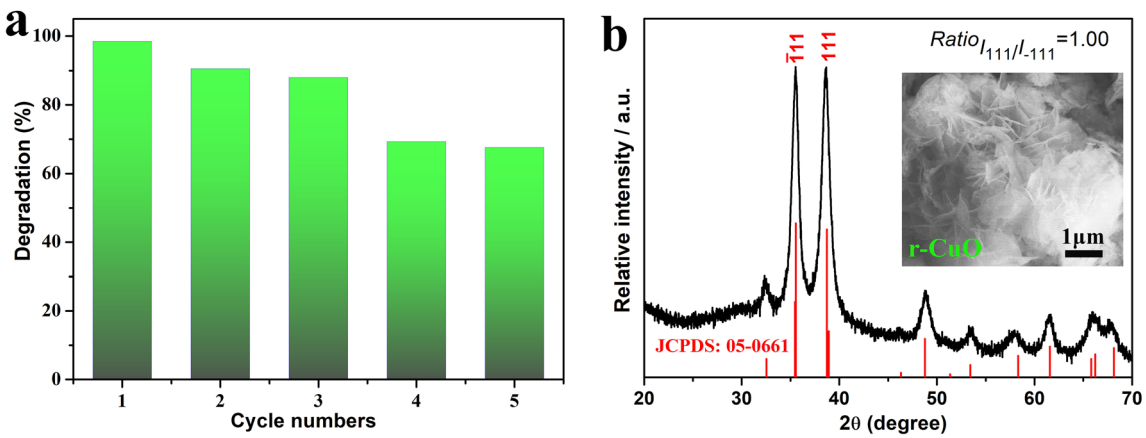

Fig. 5 **a** The profiles of five cyclic tests in the degradation of RhB over p-CuO with H_2O_2, **b** the XRD pattern and FESEM image of CuO catalyst after five cyclic tests

Scheme 2 Proposed catalytic mechanism for the p-CuO-H_2O_2 Fenton-like system

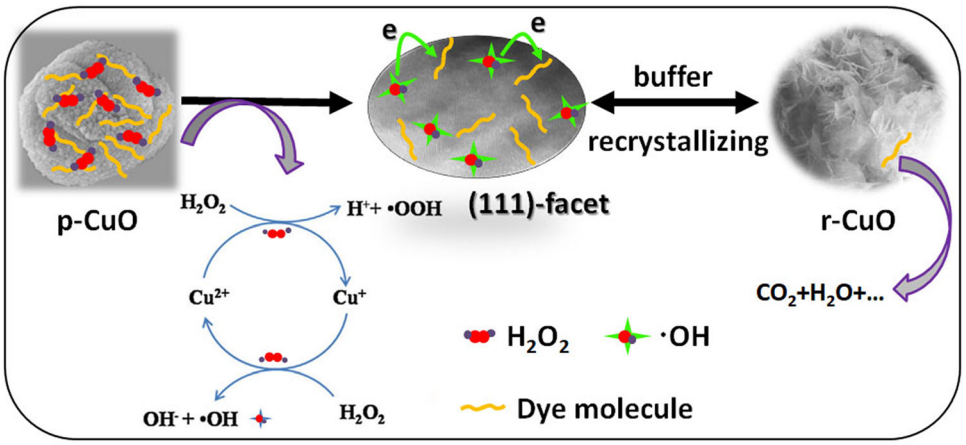

actually oxidize organic substances into inorganic minor molecules (such as CO_2, H_2O). A brief chemical catalytic reaction mechanism can be expressed as follows [43, 44]:

$$Cu^{2+} + H_2O_2 \rightarrow CuOOH^+ + H^+ \quad (6)$$

$$CuOOH^+ \rightarrow \cdot OOH + Cu^+ \quad (7)$$

$$Cu^{2+} + \cdot OOH \rightarrow Cu^+ + O_2 + H^+ \quad (8)$$

$$Cu^+ + H_2O_2 \rightarrow Cu^2 + + OH^- + \cdot OH \quad (9)$$

$$\cdot OH + \text{dyes} \rightarrow \text{degradation products} \quad (10)$$

4 Conclusions

In summary, a green convenient microwave-assisted wet chemical route has been successfully designed to controllably prepare three types of CuO architectures. The as-synthesized CuO products presented good peroxidase-like catalytic abilities in degradations of two cationic (RhB, MB) and one anionic (MO) dyes within 40 min. Significantly, p-CuO with preferential orientation of (111) crystal surface exhibited fastest and best Fenton-like catalytic properties in degradations of three types of organic dyes. It is disclosed that the peroxidase-like catalytic activity of CuO catalysts are closely relevant to the exposed (111) crystal surface. Furthermore, the present Fenton-like catalysis system was operated throughout in the dark, and no extra physical fields such as light, ultrasound, and/or microwave were applied,

suggesting a meaningful practical application in wastewater purification.

Acknowledgements

This work was supported by the Open Foundation of Anhui Province Key Laboratory of Advanced Building Materials (JZCL002KF), the Natural Science Foundation of Anhui Province (1808085MB40), the Key Projects of Research and Development Program of Anhui Provence (201904b11020040), the Natural Science Foundation of Anhui Province Educational Committee (KJ2019A0773, KJ2018A0511), and the Doctoral Foundation of Anhui Jianzhu University (2019QDZ65, 2019QDZ23).

Declarations

Conflict of interest The authors declare that they have no known competing financial interests or personal relationships that could have appeared to influence the work reported in this paper.

References

1. H. Kyung, J. Lee, W. Choi, Simultaneous and synergistic conversion of dyes and heavy metal ions in aqueous TiO_2 suspensions under visible-light illumination. Environ. Sci. Technol. **39**, 2376–2382 (2005)
2. M.A. Oturan, J.J. Aaron, Advanced oxidation processes in water/wastewater treatment: principles and applications. a review. Crit. Rev. Environ. Sci. Technol. **44**, 2577–2641 (2014)
3. R. Miao, Z. Luo, W. Zhong, S.Y. Chen, T. Jiang, B. Dutta, Y. Nasr, Y. Zhang, S.L. Suib, Mesoporous TiO_2 modified with carbon quantum dots as a high-performance visible light photocatalyst. Appl. Catal. B Environ. **189**, 26–38 (2016)
4. A. Bernabeu, S. Palacios, R. Vicente, R.F. Vercher, S. Malato, A. Arques, A.M. Amat, Solar photo-Fenton at mild conditions to treat a mixture of six emerging pollutant. Chem. Eng. J. **198–199**, 65–72 (2012)
5. E. Alfaya, O. Iglesias, M. Pazos, M.A. Sanromán, Environmental application of an industrial waste as catalyst for the electro-Fenton-like treatment of organic pollutants. RSC Adv. **5**, 14416–14424 (2015)
6. E. Neyens, J. Baeyens, A review of classic Fenton's peroxidation as an advanced oxidation technique. J. Hazard. Mater. **98**, 33–50 (2003)
7. S. Giannakis, S. Liu, A. Carratala, S. Rtimi, M.L. Bensimon, C. Pulgarin, Effect of Fe(II)/Fe(III) species, pH, irradiance and bacterial presence on viral inactivation in wastewater by the photo-Fenton process: kinetic modeling and mechanistic interpretation. Appl. Catal. B Environ. **204**, 156–166 (2016)
8. W. Luo, L. Zhu, N. Wang, H. Tang, M. Cao, Y. She, Efficient removal of organic pollutants with magnetic Nanoscaled $BiFeO_3$ as a reusable heterogeneous fenton-like catalyst. Environ. Sci. Technol. **44**, 1786–1791 (2010)
9. X.J. Yang, X.M. Xu, J. Xu, Y.F. Han, Iron oxychloride (FeOCl): an efficient Fenton-like catalyst for producing hydroxyl radicals in degradation of organic contaminants. J. Am. Chem. Soc. **135**, 16058–16061 (2013)
10. F. Chen, S. Xie, X. Huang, X. Qiu, Ionothermal synthesis of Fe_3O_4 magnetic nanoparticles as efficient heterogeneous Fenton-like catalysts for degradation of organic pollutants with H_2O_2. J. Hazard. Mater. **322**, 152–162 (2017)
11. S. Yang, W. Zhang, J. Xie, R. Liao, X. Zhang, B. Yu, R. Wu, X. Liu, H. Li, Z. Guo, Fe_3O_4@SiO_2 nanoparticles as a high-performance Fenton-like catalyst in a neutral environment. RSC Adv. **5**, 5458–5463 (2014)
12. D. Du, W. Shi, L. Wang, J. Zhang, Yolk-shell structured Fe_3O_4@void@TiO_2 as a photo- Fenton-like catalyst for the extremely efficient elimination of tetracycline. Appl. Catal. B Environ. **200**, 484–492 (2017)
13. X. Li, X. Liu, L. Xu, Y. Wen, J. Ma, Z. Wu, Highly dispersed Pd/PdO/Fe_2O_3 nanoparticles in SBA-15 for Fenton-like processes: confinement and synergistic effects. Appl. Catal. B Environ. **165**, 79–86 (2015)
14. Y. Li, W. Sun, J. Xu, B. Yuan, C. Shen, Large scale preparation of Cu-doped alpha-FeOOH nanoflowers and their photo-Fenton-like catalytic degradation of diclofenac sodium. Chem. Eng. J. **291**, 174–183 (2016)
15. Y. Yao, F. Lu, Y. Zhu, F. Wei, X. Liu, C. Lian, Wang, Magnetic core–shell $CuFe_2O_4$@C_3N_4 hybrids for visible light photocatalysis of Orange II. J. Hazard. Mater. **297**, 224–233 (2015)
16. S. Huang, Y. Xu, T. Zhou, M. Xie, Y. Ma, Constructing magnetic catalysts with in-situ solid-liquid interfacial photo-Fenton-like reaction over Ag_3PO_4@$NiFe_2O_4$ composites. Appl. Catal. B Environ. Int. J. Devoted Catal. Sci. Appl. **225**, 40–50 (2018)
17. N. Wang, T. Zheng, G. Zhang, P. Wang, A review on Fenton-like processes for organic wastewater treatment. J. Environ. Chem. Eng. **4**, 762–787 (2016)
18. T. Rhadfi, J.Y. Piquemal, L. Sicard, F. Herbst, E. Briot, M. Benedetti, A. Atlamsani, Polyol-made Mn_3O_4 nanocrystals as efficient Fenton-like catalysts. Appl. Catal. A **386**, 132–139 (2010)

19. C. Deng, X. Ge, H. Hu, L. Yao, C. Han, D. Zhao, Template-free and green sonochemical synthesis of hierarchically structured CuS hollow microspheres displaying excellent Fenton-like catalytic activities. CrystEngComm **16**, 2738–2745 (2014)
20. H. Hu, J. Wang, C. Deng, C. Niu, H. Le, Microwave-assisted controllable synthesis of hierarchical CuS nanospheres displaying fast and efficient photocatalytic activities. J. Mater. Sci. **53**, 14250–14261 (2018)
21. Y. Yao, Y. Cai, G. Wu, F. Wei, X. Li, H. Chen, S. Wang, Sulfate radicals induced from peroxymonosulfate by cobalt manganese oxides ($Co_xMn_{3-x}O_4$) for Fenton-Like reaction in water. J. Hazard. Mater. **296**, 128–137 (2015)
22. S. Pouran, A. Rahim, A.R. Abdul, W.M. Daud, Review on the main advances in photo-Fenton oxidation system for recalcitrant wastewaters. J. Ind. Eng. Chem. **21**, 53–69 (2015)
23. G.M.S. Elshafei, F.Z. Yehia, O.I.H. Dimitry, A.M. Badawi, G. Eshaq, Ultrasonic assisted- Fenton-like degradation of nitrobenzene at neutral pH using nanosized oxides of Fe and Cu. Ultrason. Sonochem. **21**, 1358–1365 (2014)
24. R. Carta, F. Desogus, The enhancing effect of low power microwaves on phenol oxidation by the Fenton process. J. Environ. Chem. Eng. **1**, 1292–1300 (2013)
25. Y.H. Choi, D.H. Kim, H.S. Han, S. Shin, S.H. Hong, K.S. Hong, Direct printing synthesis of self-organized copper oxide hollow spheres on a substrate using copper(II) complex ink: gas sensing and photoelectrochemical properties. Langmuir ACS J. Surf. Colloids **30**, 700–709 (2014)
26. Z.Q. Yuan, Y. Wang, Y.T. Qian, A facile room-temperature route to flower-like CuO microspheres with greatly enhanced lithium storage capability. RSC Adv. **2**, 8602–8605 (2012)
27. A. Li, H. Song, W. Wan, J. Zhou, X. Chen, Copper oxide nanowire arrays synthesized by in-situ thermal oxidation as an anode material for lithium-ion batteries. Electrochim. Acta **132**, 42–48 (2014)
28. M.J. Deng, C.C. Wang, P.J. Ho, C.M. Lin, J.M. Chen, K.T. Lu, Facile electrochemical synthesis of 3D nano-architectured CuO electrodes for high-performance supercapacitors. J. Mater. Chem. A **2**, 12857–12865 (2014)
29. R. Sahay, J. Sundaramurthy, P.S. Kumar, V. Thavasi, S.G. Mhaisalkar, S. Ramakrishna, Synthesis and characterization of CuO nanofibers, and investigation for its suitability as blocking layer in ZnO NPs based dye sensitized solar cell and as photocatalyst in organic dye degradation. J. Solid State Chem. **186**, 261–267 (2012)
30. H. Shi, Y. Zhao, L. Na, W. Kai, T. Fei, Synthesis and photocatalytic activity of novel CuO cauliflowers grown from $Cu(OH)_2$. Catal. Commun. **47**, 7–12 (2014)
31. L. Zhu, H. Li, Z. Liu, P. Xia, Y. Xie, D. Xiong, Synthesis of the 0D/3D CuO/ZnO heterojunction with enhanced photocatalytic activity. J. Phys. Chem. C **122**, 9531–9539 (2018)
32. R. Wahab, S.T. Khan, S. Dwivedi, M. Ahamed, J. Musarrat, A.A. Al-Khedhairy, Effective inhibition of bacterial respiration and growth by CuO microspheres composed of thin nanosheets. Colloids Surf. B Biointerfaces **111C**, 211–217 (2013)
33. J.Y. Li, S. Xiong, J. Pan, Y. Qian, Hydrothermal synthesis and electrochemical properties of urchin-like coreshell copper oxide nanostructures. J. Phys. Chem. C **114**, 9645–9650 (2010)
34. X. Yu, W. Zhao, R. Xu, H. Wang, T. Liang, Hydrothermal synthesis of well-crystallized CuO hierarchical structures and their direct application in high performance lithium-ion battery electrodes without further calcination. RSC Adv. **6**, 96882–96888 (2016)
35. A. Liu, X. Zhang, J. Mu, H. Che, Synthesis of novel hollow copper oxide micro-flowers assembled by nanoparticles and their improved catalytic performances for the synthesis of organosilane. Nano Brief Rep. Rev. **11**, 1650032 (2016)
36. C. Kong, J. Lv, X. Hu, N. Zhao, K. Liu, X. Zhang, G. Meng, Z. Yang, S. Yang, Template- synthesis of hierarchical CuO nanoflowers constructed by ultrathin nanosheets and their application for non-enzymatic glucose detection. Mater. Lett. **219**, 134–137 (2018)
37. Q. Zhao, G. Ma, C. Zhai, X. Yang, M. Zhang, Facile synthesis of nanosheets-assembled hierarchical copper oxide microspheres and their ethanol gas sensing properties. New J. Chem. **41**, 15042–15048 (2017)
38. C. Deng, H. Hu, X. Ge, C. Han, D. Zhao, G. Shao, One-pot sonochemical fabrication of hierarchical hollow CuO submicrospheres. Ultrason. Sonochem. **18**, 932–937 (2011)
39. A. Angı, D. Sanlı, C. Erkey, ö Birer, Catalytic activity of copper (II) oxide prepared via ultrasound assisted Fenton-like reaction. Ultrason. Sonochem. **21**, 854–859 (2014)
40. Y. Zhang, J. He, R. Shi, P. Yang, Preparation and photo Fenton-like activities of high crystalline CuO fibers. Appl. Surf. Sci. **422**, 1042–1051 (2017)
41. C. Deng, X. Tian, Facile microwave-assisted aqueous synthesis of CdS nanocrystals with their photocatalytic activities under visible lighting. Mater. Res. Bull. **48**, 4344–4350 (2013)
42. C.Y. Toe, Z. Zheng, H. Wu, J. Scott, R. Amal, Y.H. Ng, Photocorrosion of cuprous oxide in hydrogen production: rationalising self-oxidation or self-reduction. Angew. Chem. **130**, 13801–13805 (2018)
43. L. Zhang, X. Hai, C. Xia, X.W. Chen, J.H. Wang, Growth of CuO nanoneedles on graphene quantum dots as peroxidase

mimics for sensitive colorimetric detection of hydrogen peroxide and glucose. Sens. Actuators B **248**, 374–384 (2017)
44. L. Mi, W. Wei, Z. Zheng, Y. Gao, Y. Liu, W. Chen, X. Guan, Tunable properties induced by ion exchange in multilayer intertwined CuS microflowers with hierarchal structures. Nanoscale **5**, 6589–6598 (2013)